

Article

Incep-FrictionNet-Based Pavement Texture Friction Level Classification Prediction Method

Guomin Xu ¹, Xiuquan Lin ^{2,3}, Shifa Wang ¹, You Zhan ^{2,3,*} , Jing Liu ¹ and He Huang ¹

¹ Sichuan Chengmian Cangba Highway Co., Ltd., Chengdu Branch, Chengdu 610000, China; cmcbxuguomin@163.com (G.X.); cmcbhuanghe@163.com (H.H.)

² School of Civil Engineering, Southwest Jiaotong University, Chengdu 610031, China

³ Highway Engineering Key Laboratory of Sichuan Province, Chengdu 610031, China

* Correspondence: zhanyou@swjtu.edu.cn; Tel.: +86-13699442100

Abstract: Pavement skid resistance is crucial for driving safety, and pavement texture significantly impacts skid resistance performance. To realize the application of pavement texture data in assessing pavement skid resistance performance, this paper proposes a convolutional neural network model based on the InceptionV4 module to predict the pavement friction level from the pavement texture dataset. The surface texture data of indoor test-rutted slabs were collected using a portable laser scanner. The surface friction coefficient of rutted slabs was measured using a pendulum tribometer. After data pre-processing, a total of nine types of texture data that are in the range of 0.4 to 0.8 skid resistance levels are selected at an interval of 0.05 for training, validation, and testing of the network model. The same dataset and training parameters were also used to train a conventional convolutional network model for comparison. The results showed that the proposed network model achieved 97.89% classification accuracy on the test set, which was 11.94 percentage points higher than the comparison model. This demonstrates that the proposed model in this paper can evaluate pavement friction levels by non-contact scanning of textures and has higher evaluation accuracy.

Keywords: pavement texture; skid resistance prediction; inceptionv4 model; deep learning



Citation: Xu, G.; Lin, X.; Wang, S.; Zhan, Y.; Liu, J.; Huang, H. Incep-FrictionNet-Based Pavement Texture Friction Level Classification Prediction Method. *Lubricants* **2024**, *12*, 8. <https://doi.org/10.3390/lubricants12010008>

Received: 27 November 2023

Revised: 15 December 2023

Accepted: 22 December 2023

Published: 28 December 2023



Copyright: © 2023 by the authors. Licensee MDPI, Basel, Switzerland. This article is an open access article distributed under the terms and conditions of the Creative Commons Attribution (CC BY) license (<https://creativecommons.org/licenses/by/4.0/>).

1. Introduction

Pavement skid resistance is an essential indicator for evaluating the safety risk of roadway traffic [1,2]. Most traffic accidents are related to the decline in the anti-skid performance of road surfaces. Previous research shows that improving roadway skid resistance by 10% reduces traffic accident rates by 13% [3]. The anti-skid performance of pavement is related to the surface texture structure. The Permanent International Association of Road Congresses (PIARC) classifies texture according to wavelength and amplitude into micro-texture ($\lambda < 0.5$ mm, $h < 0.2$ mm), macro-texture (0.5 mm $< \lambda < 50$ mm, 0.2 mm $< h < 10$ mm), coarse texture (50 mm $< \lambda < 500$ mm, 0.5 mm $< h < 50$ mm), and unevenness (500 mm $< \lambda$) [4]. The macro- and micro-textures of the pavement provide the vehicle with the primary anti-skid properties. According to a mechanical point of view, road friction is the result of the interaction between adhesion and hysteresis. The micro-texture mainly affects the adhesion component and provides the anti-skid performance of the vehicle under low-speed driving conditions. The macro-texture mainly affects the hysteresis component, providing the anti-skid performance of the vehicle under high-speed driving conditions and timely draining water existing on the road surface. Macrotexture and microtexture can be characterized by direct or indirect measurements [5]. Macrotexture is usually characterized by mean texture depth (MTD) and mean profile depth (MPD) [6]. The traditional method of measuring MTD is mainly the sand patch method. The pendulum value measured by the British Pendulum Tester (BPT) system is usually used to indirectly characterize the pavement microtexture, and its measurement speed is about 10 km/h. Research has proven that microtexture has a great impact on anti-skid performance at

low speeds [7]. These methods are all fixed-point detection methods, which have the disadvantage of hindering traffic flow and have low detection efficiency. Lateral force test vehicles, wheel lock testers, variable slip devices, and other equipment can directly measure the friction coefficient and achieve road network-level measurements. However, testing is expensive due to test tire wear caused by continuous contact collection [8]. Therefore, evaluating the anti-skid performance of pavement through non-contact methods has become a research hotspot for many scholars. In other words, establishing the relationship between pavement texture and skid resistance requires obtaining a large amount of texture data.

With the development of high-precision non-contact laser scanning technology and improved computing power, researchers have used non-contact scanning equipment to obtain pavement texture information. They utilized various technical methods of texture characterization to establish a connection with the pavement's anti-skid performance. Previous studies acquired pavement texture information by the laser scanner and extracted macro and micro texture feature parameters from the perspective of spatial texture parameters [9–11]. Multivariate regression analysis was performed using these parameters and pavement skid resistance measures like BPN, friction coefficient, and grip test values [12]. This enabled the development of models to predict pavement skid resistance. However, there are omissions in the selection of feature parameters in the linear regression model, which limits the model's generalization ability. Leveraging previous works, scholars have extracted more categories of 3D texture parameters to assess pavement skid resistance performance by machine learning methods such as Random Forest (RF), Gradient Boosting Decision Tree (GBDT), Extreme Gradient Boosting (XGBoost), Light Gradient Boosting Machine (Light-GBM), Feed-forward Neural Network, etc. [13–15]. Some scholars also processed the pavement texture data from the perspective of a signal system and characterized it by the 2D wave spectrum and power spectral density (PSD) [16–19]. Several studies have characterized the skid resistance of asphalt mixture aggregates in terms of fractal dimension as well as multiple fractal spectral features [20–23]. Nevertheless, there are still some limitations to assessing pavement anti-skid performance. Machine learning models require less configuration of layer numbers, but all data must go through tedious manual feature extraction before being input. With recent advances in deep learning and convolutional neural networks, input data can undergo multilayer nonlinear transformations for adaptive feature extraction. Such deep learning models have demonstrated considerable benefits in diverse application areas. Tong et al. [24] trained a deep learning model based on a convolutional neural network to predict the MTD value from the collected pavement texture data. The results showed that the model's prediction error was lower than that of the traditional manual sand patch test. However, the MTD value only reflects the macrotexture level of the surface texture, and the correlation coefficients with the pavement skid resistance indexes, such as the SFC value, are not significant [25]. A study by Yang et al. [26] introduced a convolutional neural network model named FrictionNet. This model transforms 3D texture data into spectrograms, eliminating the need for pre-extracted texture parameters. It directly inputs them into the model training to realize the classification and evaluation of pavement skid resistance. However, the model's shallow depth with few layers restricts its ability to extract complex features.

The road surface anti-skid performance prediction model based on machine learning is mainly a regression model. Various characteristic parameters of the pavement texture and factors affecting the anti-skid performance of the surface are taken as input, and the specific road friction coefficient is provided as the output. There are also machine-learning anti-skid performance evaluation models based on classification tasks [27]. However, the number of data sets for such models are not large, which limits the model's ability to evaluate anti-skid performance. The road surface anti-skid performance prediction model based on deep learning technology is mainly a qualitative classification model. The road texture are converted into image data as input, and the corresponding friction classification level is provided; that is, it is in a certain friction coefficient range. In the process of anti-skid performance evaluation at the road network level, road engineering maintenance experts

need to quickly evaluate whether a certain road section needs repair or maintenance. The anti-skid prediction model based on classification tasks is more suitable for experts.

This study was inspired by GoogleNet [28], which built the Inception module and demonstrated powerful feature extraction capabilities, amazing classification accuracy in ImageNet, and challenging classification tasks. The purpose of this study is to build a deep learning model based on the Inception V4 module [29] that specifically uses road surface texture data to directly predict friction levels. This model combines small-size convolution kernels and asymmetric convolution kernels to extract texture features and classification boundaries at different scales. Not only can the network depth be increased, but it can also have stronger feature extraction capabilities, thus improving the prediction accuracy of the anti-skid level. This study used sufficient data sets to train, verify, and test the built model, namely 155,648 pairs of texture and anti-skid data sets collected from indoor experiments.

The remainder of this paper can be summarized as follows: Section 2 introduces the main structure of the proposed network model and the overall workflow. Section 3 describes the collection and preprocessing processes of the dataset. Section 4 analyzes and discusses the process and evaluation results of model training. Our conclusions are summarized in Section 5.

2. Model Introduction

2.1. Inception Module

The Inception module utilizes a convolutional neural network (CNN) architecture. In contrast to traditional CNNs, it concurrently applies convolutional kernels of different sizes in a single layer. A pooling operation aggregates their outputs, enabling the network to extract multi-scale features per layer. This helps capture local and global patterns in the input image [28]. Before performing large-size convolutional kernel computation, the Inception module applies 1×1 kernels to reduce input feature map channels. This decreases model parameters while still obtaining a larger receptive field to extract richer features. Traditional CNN architectures apply just one convolution or pooling operation per layer to extract features. Stacking many such layers risks overfitting, despite increasing depth. In this paper, two basic modules of InceptionV4 are selected as the feature extraction module for pavement texture data, and their basic structures are shown in Figures 1 and 2, respectively.

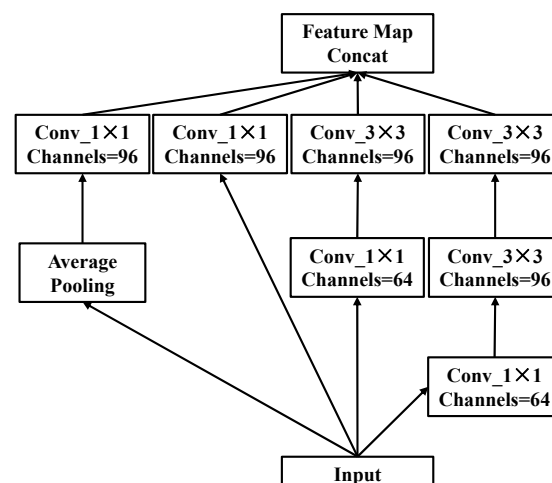


Figure 1. Inception A module.

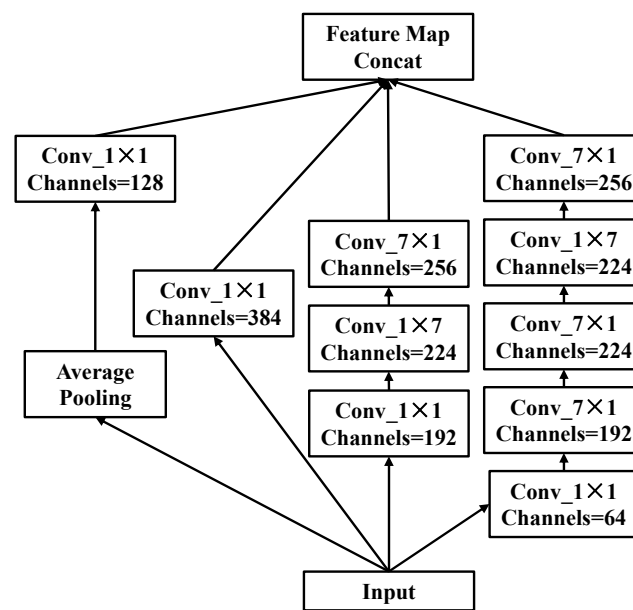


Figure 2. Inception B module.

The Inception A module replaces the 5×5 convolution kernel in the original module with two 3×3 convolution kernels. It also applies 1×1 convolution kernels to reduce channels and computations. The Inception B module utilizes asymmetric convolution kernels rather than large symmetric kernels. Specifically, it applies 1×7 and 7×1 convolution kernels instead of 7×7 convolution kernels. In both Inception A and B modules, the convolved feature maps from different kernel sizes are stacked and then fused via pooling operations.

2.2. Incep-FrictionNet Network Architecture

Since InceptionV4 targets image classification for ImageNet, it does not apply to this paper's pavement texture dataset. By incorporating Inception A and B modules, a new Incep-FrictionNet is proposed for predicting anti-skid levels from pavement textures. Figure 3 shows the network architecture. The input texture data undergoes initial processing in the backbone feature extraction network. This step aims to capture the shallow features present in the pavement texture data. Subsequently, the data passes through four Inception A modules, each with a consistent structure, followed by seven Inception B modules employing a uniform structure. This process is designed to extract deep features at various scales. The Inception A and Inception B modules exclusively modify the number of channels within the feature layer without altering the size of the feature layer itself. Downsampling is conducted individually after the final Inception A module and the concluding Inception B module. In this process, a 3×3 convolution kernel with a stride of 2 is employed, along with the integration of a maximum pooling layer, to effectively diminish the feature size. In the final stage, following the global average pooling layer for the flattening of deep features, the process proceeds to the fully connected layer. Subsequently, the output corresponds to the anti-skid level classification of the texture data, achieved through the activation function. The number of neurons in the fully connected layer aligns with the quantity of anti-skid-level classifications. To enhance training convergence speed, batch normalization and ReLU activation functions are applied after each convolution operation. This study is a multi-classification processing task, and the final output uses the Softmax activation function. This activation function expresses the output of the sample as the probability of belonging to a certain category, as shown in Equation (1). Batch normalization and ReLU activation functions are performed after each convolution operation to speed up training convergence. Batch normalization normalizes the output of each batch of data after the convolution operation [30]. Normalize the sample to a distribution with a mean

of 0 and a variance of 1 to stabilize the calculation, as shown in Equation (2). The ReLU activation function [31] is used to prevent the weight gradient from disappearing, as shown in Equation (3).

$$P(y = j|z(i)) = \frac{e^{z_j(i)}}{\sum_{j=0}^k e^{z_k(i)}} \quad (1)$$

where $z_j(i)$ is the output of the i th sample corresponding to the j th category. There are $k + 1$ categories in total. The sample output is finally converted into the probability of belonging to the j th category.

$$\hat{x}_i = \gamma \frac{x_i - \mu_b}{\sqrt{\sigma_b^2 + \varepsilon}} + \beta \quad (2)$$

where x_i is a sample in a batch, μ_b is the sample mean in a batch, σ_b is the corresponding standard deviation, ε is a very small constant, and γ and β are trainable parameters.

$$\text{ReLU}(x) = \begin{cases} 0, & \text{if } x < 0 \\ x, & \text{if } x \geq 0 \end{cases} \quad (3)$$

where x is the input sample matrix.

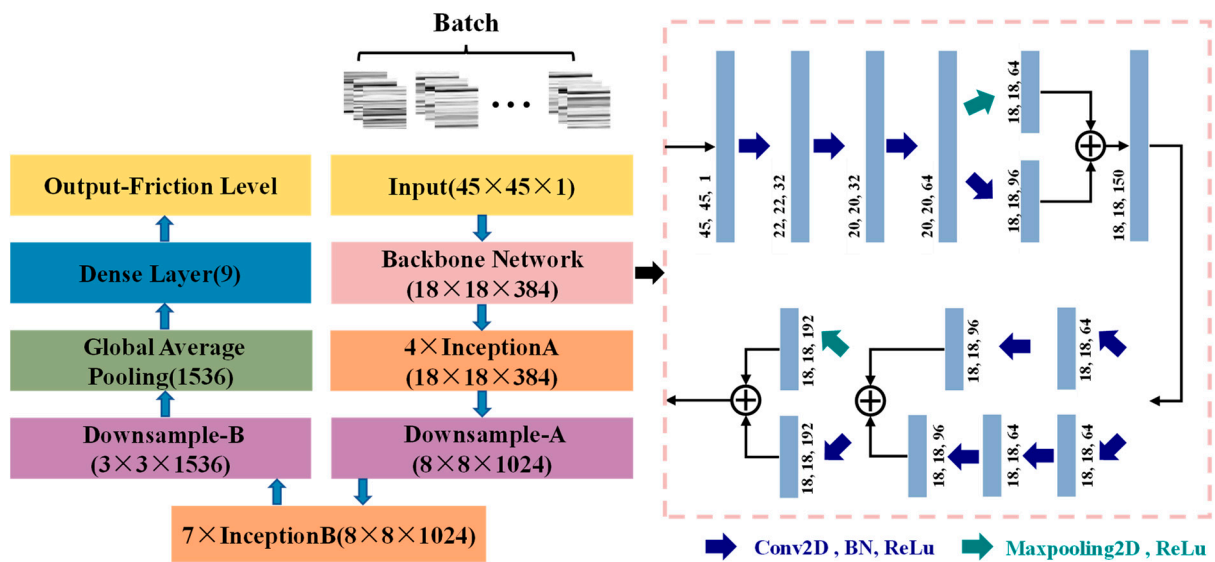


Figure 3. The Incep-FrictionNet architecture.

2.3. Overall Methodological Flow

The comprehensive workflow encompasses several key stages: data acquisition for both texture data and skid resistance level classification; noise removal from the texture data; conversion of texture data into texture-gray scale maps; partitioning of the dataset; and the subsequent phases of network model training and validation testing. The corresponding flow chart is depicted in Figure 4. The training set is input into the Incep-FrictionNet for training, and the loss function is recorded to judge the convergence of the model. The validation set is used to evaluate whether there is an overfitting risk in the model, and the test set is used to judge the model's Generalization Ability.

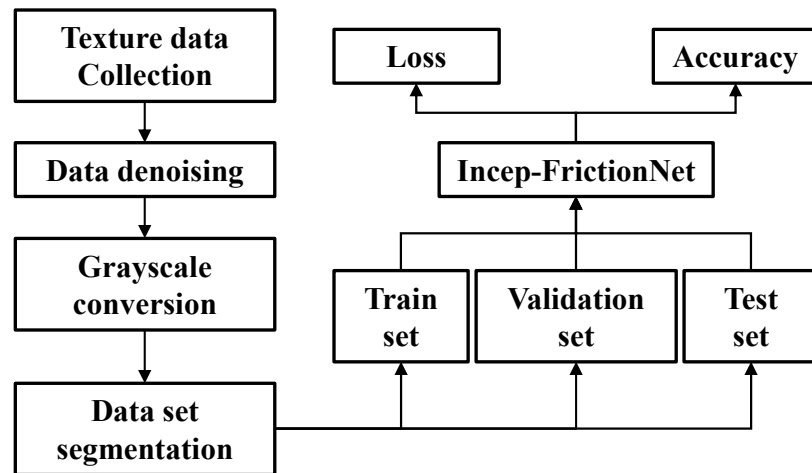


Figure 4. Flowchart for predicting skid resistance level based on a textured dataset.

3. Data Acquisition and Preprocessing

3.1. Indoor Rutted Plate Specimen Data Collection

This paper collected texture data from rutted plate specimens (300 mm × 300 mm × 50 mm) molded by the free indoor wheel milling method. The aggregate type is basalt, and the gradation type of the mixture is SMA-13. Figure 5 shows the information on the SMA-13 grading curve, including the upper grading limit, the lower grading limit, and the grading median value. In this study, the asphalt mixture was formed according to the gradation median, and the optimal oil-stone ratio was 5.84%.

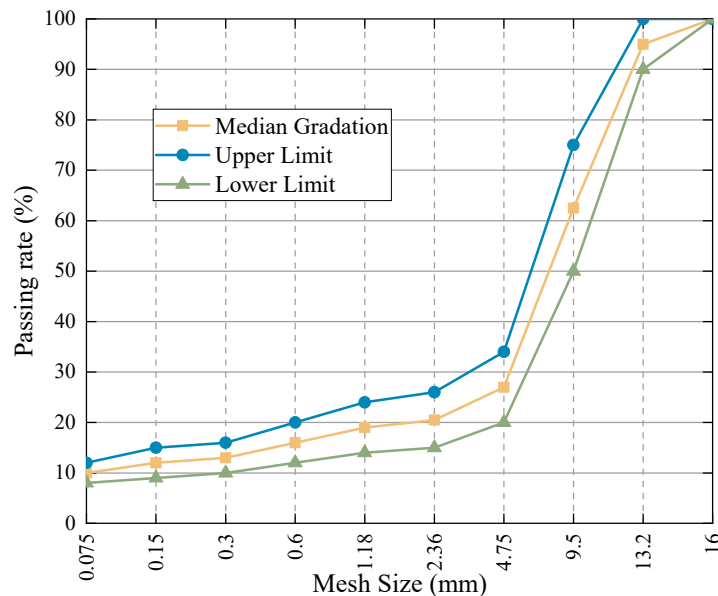


Figure 5. The gradation curves of the SMA-13 asphalt mixtures.

The formed rutted plate specimens were scanned for initial texture data on the surface of the specimen package by using a portable three-dimensional texture scanner (LS-40) [32]. Simultaneously, the BPN value was measured using a BP-III pendulum tribometer. The scanner LS-40 has a scanning resolution of 0.05 mm in the horizontal direction and 0.01 mm in the vertical direction, with a scanning area of 102.4 × 102.4 mm, and can eventually export an array of 2048 × 2048, with the values in the array representing the pixel elevation.

The BPT system, developed in the United Kingdom during the 1960s, serves as a portable friction device. Comprising a suspended pendulum, a support platform, and a

test sample, the system operates by placing the test sample horizontally on the support platform. Following the adjustment of the BPT system by the user manual, the rubber block attached to the pendulum is released from its horizontal position, initiating a swing along the fixed fulcrum. As the rubber block makes contact with the surface of the test sample at an approximate speed of 10 km/h, friction arises due to the interaction between the two surfaces. This interaction leads to the gradual dissipation of energy from the rubber block during contact. Consequently, the pendulum decelerates, eventually coming to a complete stop due to the effects of friction. By quantifying the swing angle of the pendulum following contact, the British Pendulum Number (BPN) can be determined [33]. The BPN value can be converted into a friction coefficient, which represents the tire-road friction force. In this study, the BM-III pendulum friction meter was employed for fixed-point testing of the surface friction coefficient in rough asphalt mixture specimens. The testing procedures adhere to the specification (JTG 3450-2019 [34]). During the measurement of each test sample, the pendulum meter undergoes a sequence of steps, encompassing instrument leveling, pointer zeroing, and calibration of the sliding length. Specifically, gently release the pendulum from the left and right sides, respectively, so that the edge of the rubber block comes into contact with the surface. Change the height of the pendulum by turning the lifting knob, adjusting the distance between the two contact points (i.e., the sliding length), and referring to the standard ruler to ensure that the distance between the two points meets the specification requirements, that is, $126 \text{ mm} \pm 6 \text{ mm}$. Before releasing the pendulum from the horizontal position, employ a dry brush to cleanse the specimen's surface of any contaminants. Subsequently, utilize a water spray bottle to moisten the surface of the object under investigation. Following this, employ a thermometer to gauge the temperature of the wet specimen surface. Finally, release the pendulum to measure the BPN value. Repeat the pendulum release operation five times, recording the pendulum value for each test. Among the five swing values, it is specified that the difference between the maximum and minimum values should not exceed 3. If the difference surpasses 3, repeat the aforementioned operations until the stipulated requirements are met. The average of the five specified swing values serves as the measurement result of BPN_T at the corresponding temperature. Calculate the pendulum value BPN_{20} at the standard temperature of $20 \text{ }^\circ\text{C}$ according to Equation (4) and use it as the ultimate measured friction value (all subsequent references to BPN values signify the BPN_{20} value).

$$BPN_{20} = BPN_T + \Delta BPN \quad (4)$$

where BPN_{20} denotes the swing value at the standard temperature of $20 \text{ }^\circ\text{C}$; BPN_T signifies the swing value measured when the surface temperature is $T \text{ }^\circ\text{C}$; and ΔBPN represents the temperature correction value, which is chosen by Table T 0964-2 specified in the specification (JTG 3450-2019).

After every 20,000 cycles of accelerated loading abrasion on the rutted plate, the corresponding friction coefficient was recorded using a BP-III pendulum tribometer. Rutted plates undergo 200,000 cycles of abrasion, and Figure 6 shows the process of acquiring test data. In this paper, 76 sets of texture data with BPN values in the range of 40 to 80 were finally developed. The BPN ranges were preliminarily classified at intervals of 5 BPN points, and the classification number was set as the label for subsequent input to the training of the neural network model. Table 1 shows the range split, sample size, and classification labels. According to the principle of balanced classification, ten groups of samples should have been taken for each category. However, in this paper, the BPN value of the molded rutted plate specimens rarely exceeded 77.5. After 200,000 cycles of abrasion on the rutted plate specimens, only three groups of samples exhibited BPN values below 42.5. To preserve the difficulty of the categorization task as well as the variety of species, both of these samples are still retained in this paper.

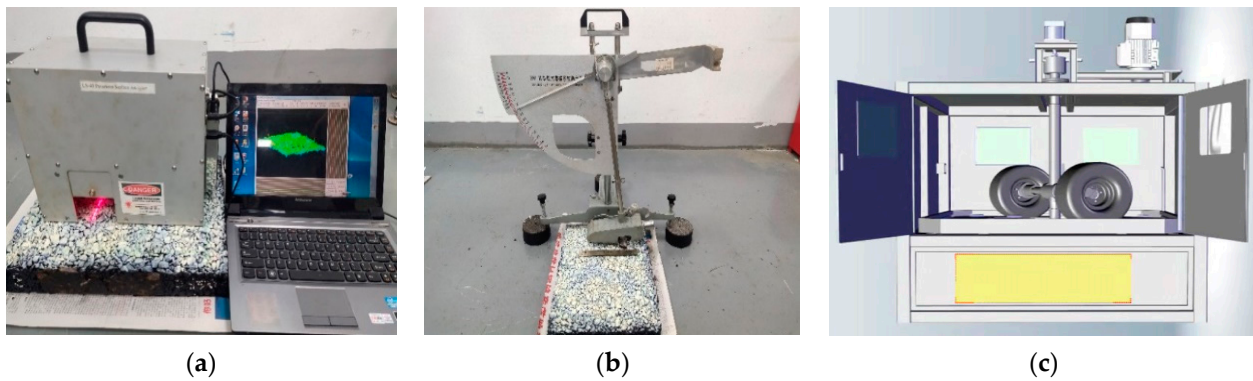


Figure 6. Data Acquisition Processes. (a) Texture scanning; (b) British Pendulum Number (BPN) Measurement; (c) Accelerated loading abrasion device.

Table 1. Anti-skid levels correspond to different BPN ranges.

BPN Ranges	Median	Number of Samples	Classification Label
[37.5,42.5)	40	3	0
[42.5,47.5)	45	10	1
[47.5,52.5)	50	10	2
[52.5,57.5)	55	10	3
[57.5,62.5)	60	10	4
[62.5,67.5)	65	10	5
[67.5,72.5)	70	10	6
[72.5,77.5)	75	10	7
[77.5,82.5)	80	3	8

3.2. Data Preprocessing

3.2.1. Texture Data Noise Reduction

Since there are outliers in the original surface texture scanned by the portable 3D texture scanner LS-40, which are generally manifested as ratio outlier noise and impulse noise representing localized texture spikes, it is necessary to remove noise from the original texture.

(1) Outlier noise removal

Outlier noise is usually caused by the portable 3D texture scanner during the scanning process due to reflections and occlusions on the surface of the object being measured, resulting in the point elevation being miscalculated. Therefore, outliers should be removed first during data preprocessing. This type of noise is generally one order of magnitude larger than the elevation value of the standard original texture, as shown in Figure 7. In this paper, the outlier noise is eliminated using the thresholding method, as illustrated by Equation (5). Since macrotexture refers to the pavement shape with heights ranging from 0.5 mm to 20 mm [35], the portable 3D texture used in this paper has a resolution of 0.01 mm in the elevation direction, the threshold value is set to 2000, and the points judged as outliers are replaced by averaging the pixel elevation.

$$\bar{H}(i,j) = \begin{cases} \text{mean} & \text{if } H(i,j) > T \\ H(i,j) & \text{else} \end{cases} \quad (5)$$

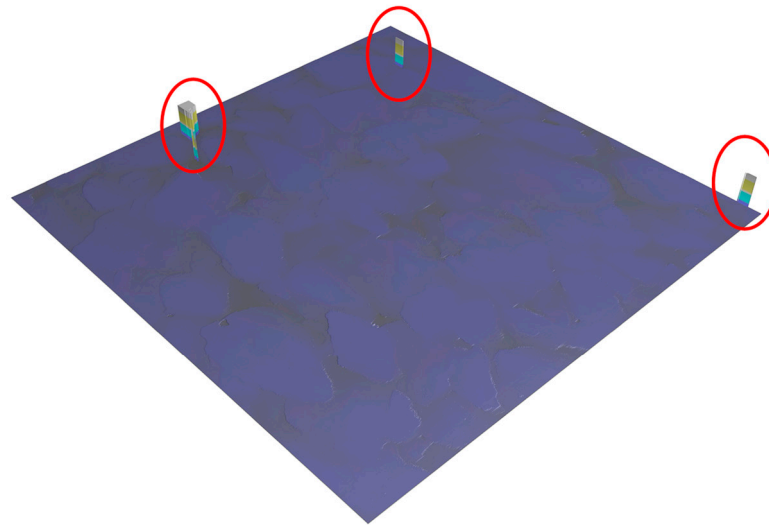


Figure 7. Original texture with outlier noise.

(2) Median Absolute Deviation (MAD) Denoising Method

After replacing the above obvious outliers using the mean value, the surface texture still has more impulse noise. Within this paper, the removal of impulse noise is accomplished through the application of the median absolute deviation method with a sliding window, as delineated in Equation (6). The window length is set as 6, n is set as 3, and i takes values 1–6, respectively.

$$\begin{aligned} MAD &= \text{median}(|x_i - \text{median}(x)|) \\ |x_i - \text{median}(x)| &< n \times MAD \end{aligned} \quad (6)$$

The reconstructed surface texture after denoising using the median absolute deviation method is shown in Figure 8. Since this method does not have a smoothing effect on inherently spiky textures, we can find that the surface consistency still has a small number of spikes locally. It is just a matter of replacing the more prominent local tip outliers through a dynamic window.

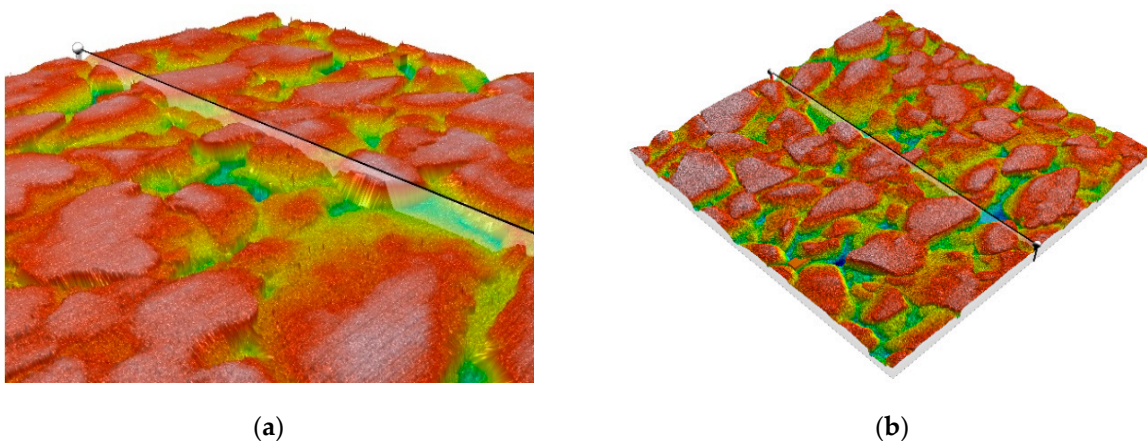


Figure 8. Cont.

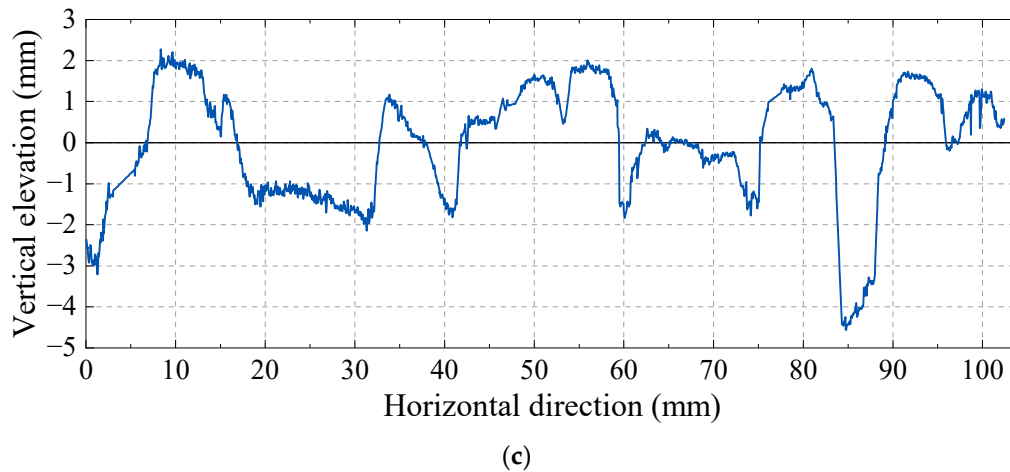


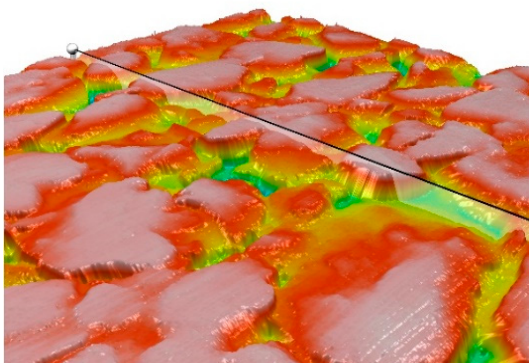
Figure 8. Texture is reconstructed after denoising by the threshold method and the MAD method. (a) partial perspective; (b) overall perspective; (c) single texture.

Where, the single texture in subfigure (c) comes from the black line labeled in subfigure (b), the zero scale line on the y-axis in subfigure (c) represents the average elevation of the texture.

(3) The Gaussian filtering method

The Gaussian filtering method can smooth the texture matrix with the expression shown in Equation (7) [36]. The process involves sliding a convolution kernel of a specific size over the texture matrix. The parameters of the convolution kernel are determined by Equation (7), which defines the weight parameters. The values of the texture matrix are then replaced through the convolution calculation, ultimately achieving the effect of smoothing. The reconstructed surface texture after denoising by Gaussian filtering is shown in Figure 9. It can be seen that the spiky noise has been removed from the surface texture compared to Figure 7.

$$G(x, y) = \frac{1}{2\pi\rho^2} e^{-(x^2+y^2)/(2\sigma^2)} \quad (7)$$



(a)



(b)

Figure 9. Cont.

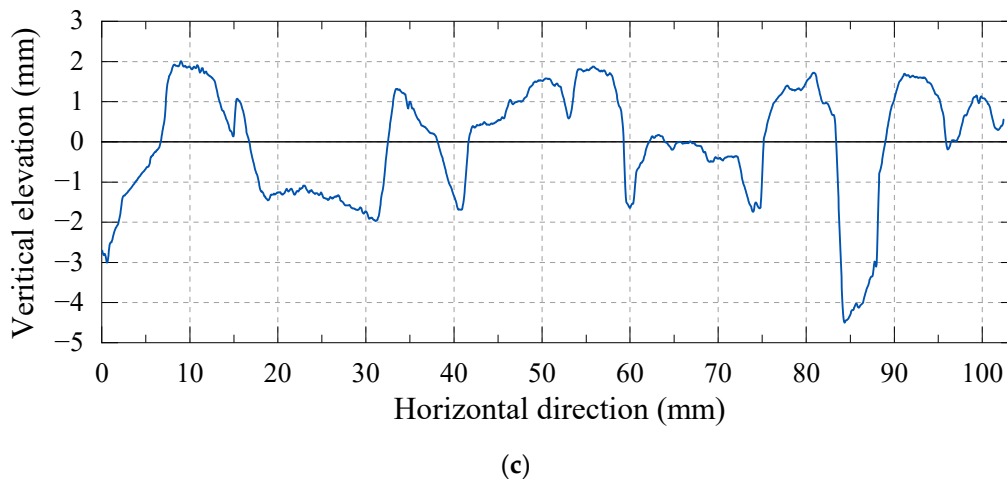


Figure 9. Texture reconstructed after Gaussian filtering based on Figure 7. (a) partial perspective; (b) overall perspective; (c) single texture.

Where, the single texture in subfigure (c) comes from the black line labeled in subfigure (b), the zero scale line on the y-axis in subfigure (c) represents the average elevation of the texture.

3.2.2. Segmentation of Data Samples

Due to the sparsity in the number of selected texture data samples in this paper, which consists of 76 groups, and each group's representatives having a size of 2048×2048 , the samples are not suitable for direct utilization as input for the neural network model due to their excessively large size and relatively small data volume. Therefore, it is imperative to segment the texture data samples after noise removal. In this study, each set of texture data with a size of 2048×2048 are divided into multiple pieces of texture data with a size of 1×2048 along the non-driving direction. As the asphalt concrete specimen is being worn, the tires in the wearing equipment roll cyclically in one direction on the surface of the specimen plate. We specify this direction as the standard direction to simulate the driving direction. Therefore, when measuring the anti-slip value using the BPT system, the rubber block slides on the surface of the specimen in the specified direction. The final segmented texture is consistent with the specified direction in the dimensional direction. For example, the positive direction of the horizontal axis in Figure 9c is the specified direction. Splitting the texture data according to the above rules can obtain 155,648 samples. This is essentially a method of data dimensionality reduction to expand the amount of data and reduce computing resources to ensure the robustness of the model. The one-dimensional texture data are transformed into a two-dimensional gray-scale image of size 45×45 . It is used to input the neural network model after min-max normalization by Equation (8).

$$\bar{x} = \frac{x - x_{\min}}{x_{\max} - x_{\min}} \quad (8)$$

4. Results and Discussions

4.1. Model Parameter Settings

We developed an Incep-FrictionNet convolutional neural network model program using Python 3.8.10 within the VsCode integrated development environment. The program utilizes the TensorFlow 2.5.0 architecture and is configured to run on a server equipped with a 16-core Intel Xeon Platinum 8350C CPU. For accelerated computation, an RTX A5000 GPU graphics card is employed. The texture dataset is divided into training sets in the proportions of 10%, 30%, 50%, and 70%, respectively. The remaining ratio is equally divided into a validation set and a test set.

The training process is preset with 100 epochs, and the number of samples in each batch is 256. The model uses the Adam optimizer to compute the gradient of the loss function and

initializes the learning rate to 5×10^{-4} . Since the prediction task is a multi-categorization task, the Sparse Categorical Cross Entropy Loss Function (SCELF) is adopted, as shown in Equation (9). To judge whether the model has the risk of overfitting, the validation set is input into the network for validation after every five epochs of training, and the accuracy rate is monitored to judge whether there is an overfitting phenomenon. At the same time, to determine whether the model converges, this paper sets the “early stop strategy” in the model. Simultaneously, to assess the convergence of the model, this paper implements the “early stop strategy” within the model. The monitoring content is the accuracy of the training set. If the accuracy of the training set does not show further improvement for three consecutive epochs, then the model training is halted and the optimal parameters are retained.

$$Loss = -\frac{1}{N} \sum_{i=1}^N y_{i,t} \times \log(y_{i,p}) \quad (9)$$

where N is the number of training samples, $y_{i,t}$ is the label of the measured skid resistance level of the texture data, and $y_{i,p}$ is the predicted output of the texture data.

4.2. Training Results and Analysis

In this paper, the model was trained by inputting different proportions of the training set. The change curves of the loss function, the validation set accuracy, and the test set accuracy were recorded to validate the effectiveness of the constructed pavement texture skid-resistance level prediction model, Incep-FrictionNet. These records are illustrated in Figures 10 and 11, respectively. As can be seen from the figure, the network model is convergent. With an increase in the proportion of the training set, the network model can acquire more intricate features from the texture data. This often results in convergence towards smaller values of the loss function, necessitating additional iterations and consequently leading to an extended training duration. We can find that the test set accuracy corresponding to the 10% to 30% ratio setting has the most obvious change, increasing from 83.89% to 92.75%, an increase of 8.86%. The test set accuracy corresponding to the 30% to 50% and 50% to 70% ratio settings also increased by 1.56% and 3.58%, respectively. Theoretically, the accuracy improvement of the latter should be lower than that of the former. However, our data set division are not based on the former but randomly selects a preset proportion of data from the total data set as a training set each time. Similarly, the larger the percentage of the training set, the higher the accuracy of the test set. When the proportion of the training set reaches 70%, the validation set can reach up to 97.96% accuracy during the training process. In comparison, the average accuracy of the test set under the corresponding optimal parameters can reach 97.89%.

Figure 11 summarizes the measured coefficient of friction classifications and predicted coefficient of friction classifications with different skid resistance level classifications in the test set with the highest accuracy. The values on the confusion matrix’s diagonal indicate the number of textures correctly predicted for that classification, as shown in Figure 12. For example, in the case where the actual friction coefficient is categorized as 0.45, there are a total of 3053 texture data points correctly predicted. In contrast, there are 56 texture data points incorrectly predicted for other friction coefficient classifications. A potential reason for this discrepancy lies in the fact that, despite employing three different denoising methods on the texture data in this study, there remains the likelihood of noise persisting in both the macro-texture and micro-texture when separating them from the original texture. Consequently, this residual noise may affect the accuracy of friction classification predictions. Another possible reason is that when we collect texture data for the same test slab (having experienced the abrasion process at different times), the scanning equipment has a small degree of deviation due to artificial placement.

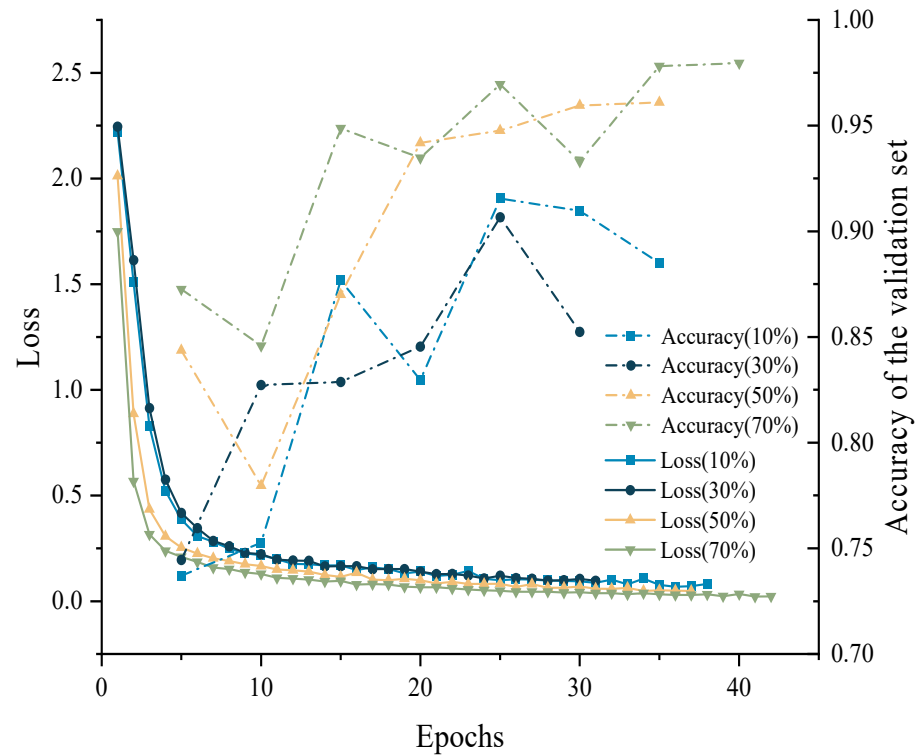


Figure 10. Change the curve of the loss value and validate the accuracy.

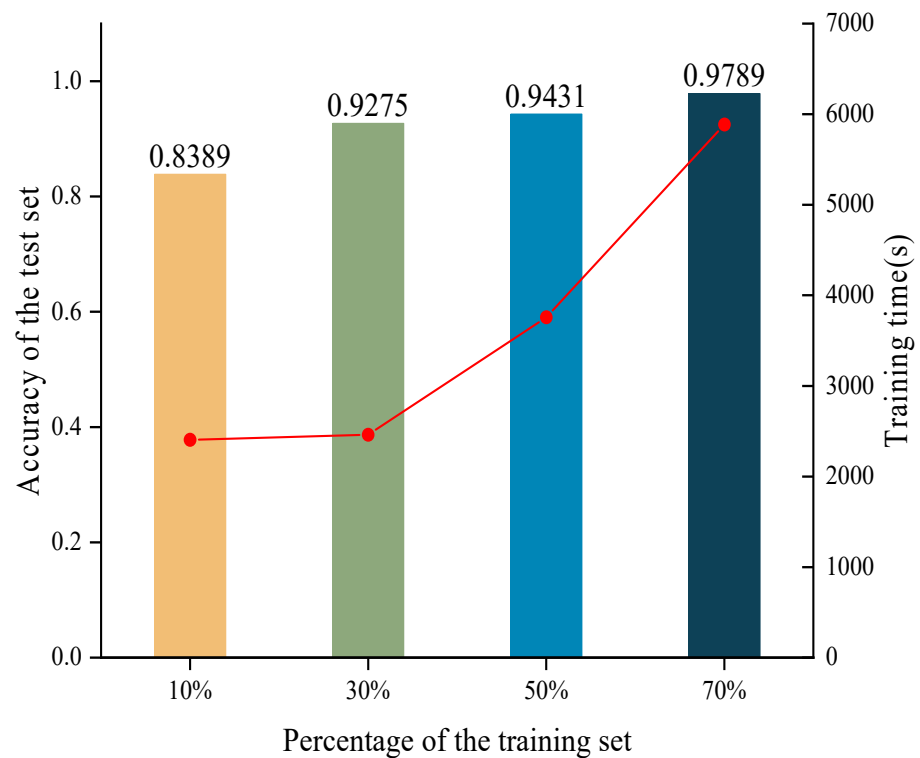


Figure 11. Test set accuracy and training time correspond to different training set proportions.

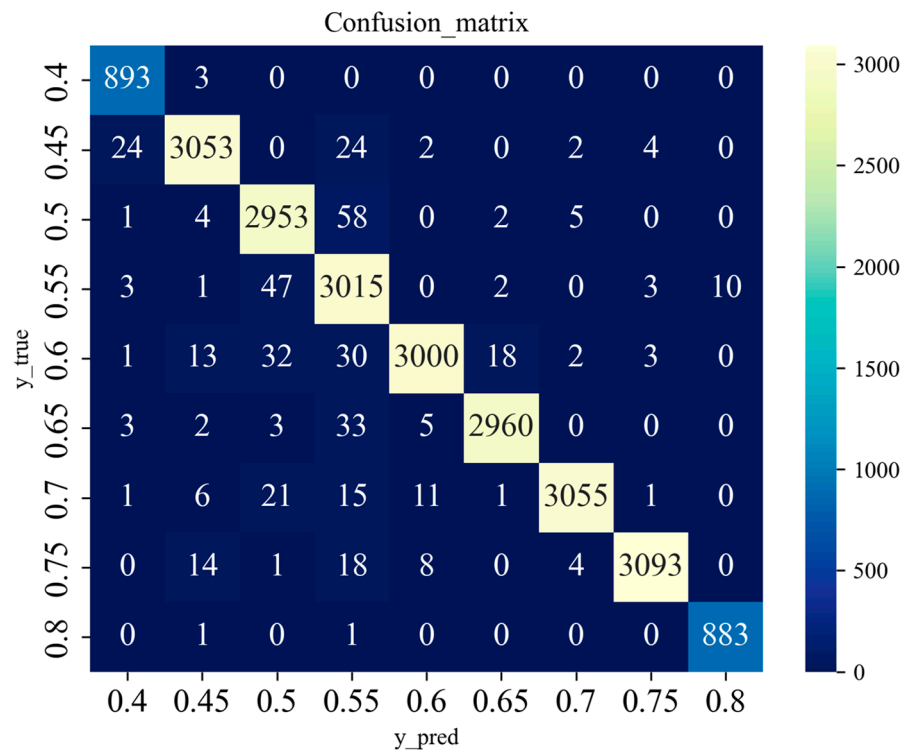


Figure 12. The confusion matrix of the test set for the best model.

4.3. Comparison of Conventional Convolutional Networks

We chose the traditional convolutional network from the literature [26] for comparison, aiming to demonstrate Incep-FrictionNet’s effectiveness further. The network mainly consists of two convolutional layers, three fully connected layers, and one output layer. Setting the batch normalization, hyperbolic tangent activation function, and one layer of average pooling operation after each pass through the convolutional layer. The Flatten operation flattens the feature map before entering the fully connected layer. A dropout rate of 0.25 is applied between the fully connected layers. L2 regularization is set to prevent overfitting, and the activation function adopts the hyperbolic tangent function to avoid gradient instability, whose expressions are as shown in Equations (10) and (11) respectively. The last output layer undergoes the SoftMax activation function to output the anti-skid level classification. Table 2 shows its structural layers and parametric quantities.

$$L2 \text{ Regularization Term} = \frac{\lambda}{2n} \sum_w \|\omega^2\| \tag{10}$$

where $\|\omega^2\|$ is the second norm of the weight parameters. The second norm of the weight parameters of all network layers is regularized as part of the loss function, and λ is a penalty factor greater than 0.

$$\tanh(x) = \frac{e^x - e^{-x}}{e^x + e^{-x}} \tag{11}$$

The “()” numbers indicate the parameters resulting from batch normalization.

The training set with a 70% proportion was fed into the comparison model for training. The initial preset hyperparameters of the model were kept consistent with the proposed network structure model. Following training, the optimal parameters were saved. Subsequently, the test set was fed into the model to calculate accuracy. As can be seen from Figure 13, the comparison model has a large number of training iterations and stops iterating at the 83rd Epoch, while the model proposed in this study reaches the best performance at the 42nd epoch under the same training configuration (as shown in Figure 10). The

final test set accuracy of the comparison model is 85.95%, which is lower than the model proposed in this study (i.e., 97.89%), as expected. Possible reasons are as follows:

- (1) The number of network layers in the comparison model is much lower than that of the model proposed in this study, which means there is a difference in the number of parameters in the network structure. Although a larger number of parameters consumes more computing resources, the model can mine the features of the input data deeper.
- (2) The comparison model only applies a symmetric convolution kernel of size 3×3 in the same layer network, which means a limited receptive field. The comparison model requires more iterations to achieve optimal performance, which also proves that the features learned by the comparison model are still not enough to finely distinguish the anti-skid level of texture data. The model proposed in this study combines asymmetric convolution kernels of different sizes and small-size convolution kernels in the same network layer. While increasing the receptive field, it also incorporates features from different angles of texture data to improve anti-skid level classification accuracy.
- (3) A sufficient amount of data were provided in this study, that is, 155,648 pairs of data samples, which are more than twice the amount of data provided by the comparison model (i.e., 63,000 pairs). Sufficient and diverse samples allow the model to learn more detailed features.

Table 2. Structure and parameters of the compared model.

Network Structure Layer	Output Size	Number of Parameters
Convolution layer_1	$43 \times 43 \times 64$	640 (256)
Average pooling layer_1	$21 \times 21 \times 64$	0
Convolution layer_2	$19 \times 19 \times 96$	55,392 (384)
Average pooling layer_2	$9 \times 9 \times 96$	0
Dense layer_1	64	497,728
Dense layer_2	96	6240
Dense layer_3	32	3104
Output_layer	9	297
Total parameters	–	564,041

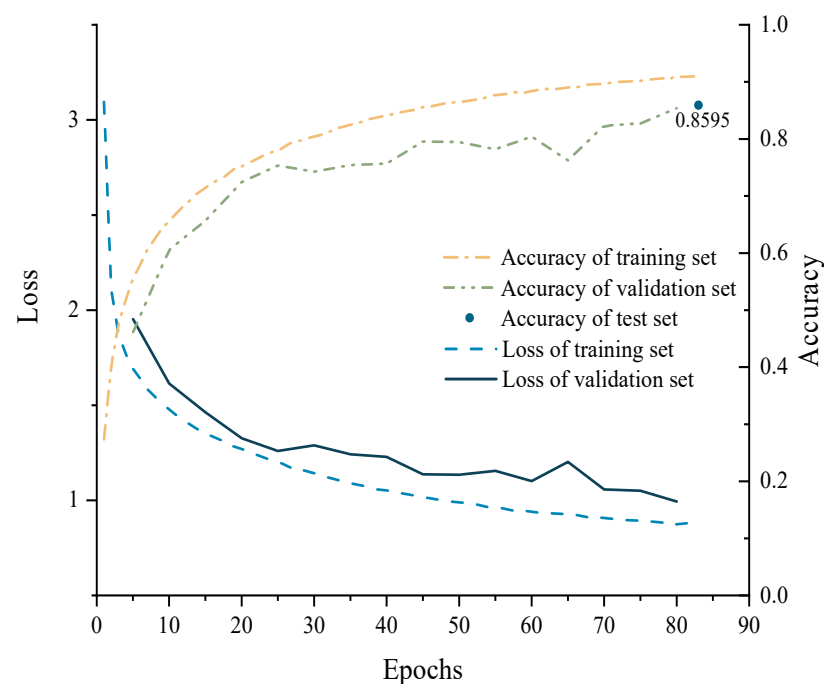


Figure 13. Loss and accuracy change curves for the compared model.

5. Conclusions

Based on the InceptionV4 module, this study builds a deep convolution model called Incep-FrictionNet based on the asphalt mixture surface texture data after noise removal preprocessing to predict the anti-skid level. After discussion and analysis, the following conclusions are drawn:

- (1) The noise removal methods proposed in this study include the threshold method, MAD method, and Gaussian filtering method. The use of these methods can filter out most of the outliers in the original pavement texture data.
- (2) For the network model constructed in this study, when the texture data training set accounts for 70%, the test set accuracy corresponding to the optimal model is 97.89%.
- (3) The network model constructed in this study achieves better performance in classifying pavement texture anti-skid levels than the traditional convolutional network model. Under the same initial training parameter configuration, the accuracy of the proposed model on the test set is 11.94 percentage points higher than that of the comparison model.

However, the method proposed in this study still has some limitations. First of all, the pavement texture data collected in this article all come from indoor experimentally molded specimens, which, to a certain extent, cannot truly simulate road surfaces that have experienced different loads and environmental effects on site. And there are omissions of texture data with extremely low anti-slip properties. In addition, when measuring the anti-skid value in this study, the temperature-corrected BPN value was used, which means that the effect of temperature was ignored. However, the non-contact skid resistance evaluation method of pavement proposed in this study is still competitive. To make the application of the model more consistent with real-life scenarios, future research will mainly include three aspects:

- (1) We will consider asphalt pavement textures of different gradation types, including texture data from the laboratory and field, and will correspond to the skid resistance level expanded to a very low anti-skid level range to help the model train better.
- (2) Consider multi-modal inputs for anti-skid performance evaluation. For the same texture data, in addition to converting it into image data as input, it also combines characteristic parameters related to anti-skid performance, representative water film thickness (representing rainfall), contact depth (representing tire action), temperature, etc. Modal parameters serve as another set of equivalent inputs to the model. The output is the anti-skid value at the road design speed.
- (3) Adopt more advanced deep learning technology.

In summary, we can use more advanced models to predict the anti-skid performance of pavement textures under various environmental effects, providing a reference for pavement maintenance management decisions.

Author Contributions: Conceptualization, G.X.; methodology, G.X. and X.L.; software, X.L., S.W., J.L. and H.H.; validation, X.L. and Y.Z.; formal analysis, X.L. and S.W.; investigation, G.X., Y.Z. and H.H.; resources, G.X.; data curation, S.W.; writing—original draft preparation, G.X., X.L. and J.L.; writing—review and editing, Y.Z.; visualization, X.L.; supervision, G.X. and Y.Z.; project administration, G.X.; funding acquisition, Y.Z. All authors have read and agreed to the published version of the manuscript.

Funding: This research was funded by [Natural Science Foundation of Sichuan Province] grant number [2022NSFSC0437].

Data Availability Statement: Due to the nature of this research, participants of this study did not agree for their data to be shared publicly, so supporting data is not available.

Conflicts of Interest: The authors declare that they have no known competing financial interests or personal relationships that could have appeared to influence the work reported in this paper.

References

1. Yu, M.; You, Z.; Wu, G.; Kong, L.; Liu, C.; Gao, J. Measurement and modeling of skid resistance of asphalt pavement: A review. *Constr. Build. Mater.* **2020**, *260*, 119878. [[CrossRef](#)]
2. Fwa, T.F. Skid resistance determination for pavement management and wet-weather road safety. *Int. J. Transp. Sci. Technol.* **2017**, *6*, 217–227. [[CrossRef](#)]
3. Ahammed, M.A.; Tighe, S.L. Early-Life, Long-Term, and Seasonal Variations in Skid Resistance in Flexible and Rigid Pavements. *Transp. Res. Rec.* **2009**, *2094*, 112–120. [[CrossRef](#)]
4. Xu, P.; Qian, G.; Zhang, C.; Wang, X.; Yu, H.; Zhou, H.; Zhao, C. Influence of the Surface Texture Parameters of Asphalt Pavement on Light Reflection Characteristics. *Appl. Sci.* **2023**, *13*, 12824. [[CrossRef](#)]
5. Chen, S.; Liu, X.; Luo, H.; Yu, J.; Chen, F.; Zhang, Y.; Ma, T.; Huang, X. A state-of-the-art review of asphalt pavement surface texture and its measurement techniques. *J. Road Eng.* **2022**, *2*, 156–180. [[CrossRef](#)]
6. Praticò, F.G.; Vaiana, R. A study on the relationship between mean texture depth and mean profile depth of asphalt pavements. *Constr. Build. Mater.* **2015**, *101*, 72–79. [[CrossRef](#)]
7. Zheng, N.; Chen, X.; Bi, J.; Wu, X. Research on the relationship between anti-skid performance and various aggregate micro texture based on laser scanning confocal microscope. *Constr. Build. Mater.* **2022**, *316*, 125984. [[CrossRef](#)]
8. Mataei, B.; Zakeri, H.; Zahedi, M.; Nejad, F.M. Pavement Friction and Skid Resistance Measurement Methods: A Literature Review. *Open J. Civ. Eng.* **2016**, *6*, 29. [[CrossRef](#)]
9. Zuniga-Garcia, N.; Prozzi, J.A. High-Definition Field Texture Measurements for Predicting Pavement Friction. *Transp. Res. Rec.* **2019**, *2673*, 15. [[CrossRef](#)]
10. Serigos, P.A.; De Fortier Smit, A.; Prozzi, J.A. Incorporating surface microtexture in the prediction of skid resistance of flexible pavements. *Transp. Res. Rec.* **2014**, *2457*, 105–113. [[CrossRef](#)]
11. Alhasan, A.; Smadi, O.; Bou-Saab, G.; Hernandez, N.; Cochran, E. Pavement friction modeling using texture measurements and pendulum skid tester. *Transp. Res. Rec.* **2018**, *2672*, 440–451. [[CrossRef](#)]
12. Jiang, T.; Ren, W.; Dong, Y.; Hou, Y.; Yuan, J. Precise Representation of Macro-texture of Pavement and Effect on Anti-skidding Performance. *J. Munic. Technol.* **2022**, *40*, 1–7+24. [[CrossRef](#)]
13. Yang, G.; Yu, W.; Li, Q.J.; Wang, K.; Peng, Y.; Zhang, A. Random forest-based pavement surface friction prediction using high-resolution 3D image data. *J. Test. Eval.* **2019**, *49*, 1141–1152. [[CrossRef](#)]
14. Zhan, Y.; Deng, Q.; Luo, Z.; Liu, C.; Zhang, A.; Qiu, Y. Research on GBDT-based skid resistance perception model for asphalt pavement. *China Civ. Eng. J.* **2023**, *56*, 121–132. [[CrossRef](#)]
15. Hu, Y.; Sun, Z.; Han, Y.; Li, W.; Pei, L. Evaluate pavement skid resistance performance based on Bayesian-LightGBM using 3D surface macrotexture data. *Materials* **2022**, *15*, 5275. [[CrossRef](#)] [[PubMed](#)]
16. Yu, M.; Kong, Y.; Wu, C.; Xu, X.; Li, S.; Chen, H.; Kong, L. The effect of pavement texture on the performance of skid resistance of asphalt pavement based on the Hilbert-Huang transform. *Arab. J. Sci. Eng.* **2021**, *46*, 11459–11470. [[CrossRef](#)]
17. Edmondson, V.; Woodward, J.; Lim, M.; Kane, M.; Martin, J.; Shyha, I. Improved non-contact 3D field and processing techniques to achieve macrotexture characterisation of pavements. *Constr. Build. Mater.* **2019**, *227*, 116693. [[CrossRef](#)]
18. Deng, Q.; Zhan, Y.; Liu, C.; Qiu, Y.; Zhang, A. Multiscale power spectrum analysis of 3D surface texture for prediction of asphalt pavement friction. *Constr. Build. Mater.* **2021**, *293*, 123506. [[CrossRef](#)]
19. Cui, Y. Study on Attenuation Law of Asphalt Pavement Anti Skid Performance Based on Fractal Theory. Master's Thesis, Chang'an University, Xi'an, China, 2018.
20. Miao, Y.; Song, P.; Gong, X. Fractal and multifractal characteristics of 3D asphalt pavement macrotexture. *J. Mater. Civ. Eng.* **2014**, *26*, 04014033. [[CrossRef](#)]
21. Liu, C.; Zhan, Y.; Deng, Q.; Qiu, Y.; Zhang, A. An improved differential box counting method to measure fractal dimensions for pavement surface skid resistance evaluation. *Measurement* **2021**, *178*, 109376. [[CrossRef](#)]
22. Zhou, X.; Xiao, S.; Liu, W.; Huang, X.; Xiao, W. Multifractal characteristics and polishing behaviors of surface texture on asphalt pavement. *J. Southeast Univ. (Nat. Sci. Ed.)* **2018**, *48*, 175–180. [[CrossRef](#)]
23. Zhou, X.; Xiao, S.; Xiao, W.; Ran, M. Multi-fractal evaluation on roughness of coarse aggregate surface texture. *J. Huazhong Univ. Sci. Technol.* **2017**, *45*, 29–33. [[CrossRef](#)]
24. Tong, Z.; Gao, J.; Sha, A.M.; Hu, L.Q.; Li, S. Convolutional Neural Network for Asphalt Pavement Surface Texture Analysis. *Comput.-Aided Civ. Infrastruct. Eng.* **2018**, *33*, 1056–1072. [[CrossRef](#)]
25. Tan, Y.; Xiao, S.; Xiong, X. Review on detection and prediction methods for pavement skid resistance. *J. Traffic Transp. Eng.* **2021**, *21*, 32–47. [[CrossRef](#)]
26. Yang, G.; Li, Q.; Zhan, Y.; Fei, Y.; Zhang, A. Convolutional Neural Network-Based Friction Model Using Pavement Texture Data. *J. Comput. Civ. Eng.* **2018**, *32*, 04018052. [[CrossRef](#)]
27. Koné, A.; Es-Sabar, A.; Do, M.-T. Application of Machine Learning Models to the Analysis of Skid Resistance Data. *Lubricants* **2023**, *11*, 328. [[CrossRef](#)]
28. Szegedy, C.; Liu, W.; Jia, Y.Q.; Sermanet, P.; Reed, S.; Anguelov, D.; Erhan, D.; Vanhoucke, V.; Rabinovich, A. Going Deeper with Convolutions. In Proceedings of the IEEE Conference on Computer Vision and Pattern Recognition, Boston, MA, USA, 7–12 June 2015; pp. 1–9. [[CrossRef](#)]

29. Szegedy, C.; Ioffe, S.; Vanhoucke, V.; Alemi, A. Inception-v4, inception-resnet and the impact of residual connections on learning. In Proceedings of the AAAI Conference on Artificial Intelligence, San Francisco, CA, USA, 4–9 February 2017. [[CrossRef](#)]
30. Loffe, S.; Szegedy, C. Batch normalization: Accelerating deep network training by reducing internal covariate shift. In Proceedings of the International Conference on Machine Learning, Lille, France, 6–11 July 2015; pp. 448–456.
31. Krizhevsky, A.; Sutskever, I.; Hinton, G.E. Imagenet classification with deep convolutional neural networks. *Adv. Neural Inf. Process. Syst.* **2012**, *25*. [[CrossRef](#)]
32. Yang, E.; Chen, Q.; Li, J.; Di, H.; Huang, B.; Qiu, Y. Surface Texture Reconstruction and MeanTexture Depth Prediction Model of Asphalt Pavement. *China J. Highw. Transp.* **2023**, *36*, 14–23. [[CrossRef](#)]
33. Pomoni, M.; Plati, C.; Loizos, A. How can sustainable materials in road construction contribute to vehicles' braking? *Vehicles* **2020**, *2*, 55–74. [[CrossRef](#)]
34. *JTG 3450-2019; Field Test Methods of Highway Subgrade and Pavement*. Ministry of Transport of the People's Republic of China: Beijing, China, 2019.
35. Shen, X.; Huang, W.; Yang, Y.; He, J.; Song, T.; Li, T. Analysis on Influencing Factors and Attenuation Law of Anti-slide Performance of Asphalt Pavement in Expressway. *Technol. Highw. Transp.* **2021**, *37*, 12–16. [[CrossRef](#)]
36. Pedregosa, F.; Varoquaux, G.; Gramfort, A.; Michel, V.; Thirion, B.; Grisel, O.; Blondel, M.; Prettenhofer, P.; Weiss, R.; Dubourg, V. Scikit-learn: Machine learning in Python. *J. Mach. Learn. Res.* **2011**, *12*, 2825–2830.

Disclaimer/Publisher's Note: The statements, opinions and data contained in all publications are solely those of the individual author(s) and contributor(s) and not of MDPI and/or the editor(s). MDPI and/or the editor(s) disclaim responsibility for any injury to people or property resulting from any ideas, methods, instructions or products referred to in the content.